# 3D Dirac semimetal Cd$_3$As$_2$: A review of material properties

I. Crassee,[1] R. Sankar,[2] W.-L. Lee,[2] A. Akrap,[3] and M. Orlita[1,4,*]

[1]*Laboratoire National des Champs Magnétiques Intenses, CNRS-UGA-UPS-INSA, 25, avenue des Martyrs, 38042 Grenoble, France*
[2]*Institute of Physics, Academia Sinica, Nankang, 11529 Taipei, Taiwan*
[3]*Department of Physics, University of Fribourg, Chemin du Musée 3, CH-1700 Fribourg, Switzerland*
[4]*Institute of Physics, Charles University, Ke Karlovu 5, 12116 Praha 2, Czech Republic*

Cadmium arsenide (Cd$_3$As$_2$), a time-honored and widely explored material in solid-state physics, has recently attracted considerable attention. This was triggered by a theoretical prediction concerning the presence of three-dimensional (3D) symmetry-protected massless Dirac electrons, which could turn Cd$_3$As$_2$ into a 3D analog of graphene. Subsequent extended experimental studies have provided us with compelling experimental evidence of conical bands in this system, and revealed a number of interesting properties and phenomena. At the same time, some of the material properties remain the subject of vast discussions despite recent intensive experimental and theoretical efforts, which may hinder the progress in understanding and applications of this appealing material. In this paper, we focus on the basic material parameters and properties of Cd$_3$As$_2$, in particular those which are directly related to the conical features in the electronic band structure of this material. The outcome of experimental investigations, performed on Cd$_3$As$_2$ using various spectroscopic and transport techniques within the past 60 years, is compared with theoretical studies. These theoretical works gave us not only simplified effective models, but more recently, also the electronic band structure calculated numerically using *ab initio* methods.

## I. INTRODUCTION

Cadmium arsenide (Cd$_3$As$_2$) is an old material for condensed-matter physics, with its very first investigations dating back to the 1930's [1]. Research on this material then continued extensively into the 1960's and 1970's, as reviewed in Ref. [2]. This is when the physics of semiconductors, those with a sizable, narrow, but also vanishing energy band gap, strongly developed.

In the early stages of research on Cd$_3$As$_2$, it was the extraordinarily high mobility of electrons, largely exceeding $10^4$ cm$^2$/(V s) at room temperature [3–5], that already attracted significant attention to this material. Even today, with a declared mobility well above $10^6$ cm$^2$/(V s) [6] at low temperatures, cadmium arsenide belongs to the class of systems with the highest electronic mobilities, joining materials such as graphene, graphite, bismuth, and two-dimensional (2D) electron gases in GaAs/GaAlAs heterostructures [7–11]. Another interesting, and in view of recent developments, crucial, observation was the strong dependence of the effective mass of electrons on their concentration, which implies a nearly conical conduction band, in other words the energy dispersion is linear in momentum (see Refs. [5,12,13] and Fig. 1).

To understand the electronic properties of Cd$_3$As$_2$, and its extraordinarily large mobility of electrons in particular, simple theoretical models for the electronic band structure have been proposed in the standard framework of semiconductors physics, and compared with optical and transport experiments. In the initial phase of research, cadmium arsenide was

treated as an ordinary Kane-type semiconductor or semimetal [14,15]. It was seen as a material with an electronic band structure that closely resembled zinc-blende semiconductors with a relatively narrow or vanishing band gap. However, no clear consensus was achieved concerning the particular band structure parameters (Refs. [2] or [16]). Most notably, there was disagreement about the ordering of electronic bands and the presence of another conduction band at higher energies.

Renewed interest in the electronic properties of Cd$_3$As$_2$ was provoked by a theoretical study where Wang *et al.* [17] invoked the presence of a pair of symmetry-protected three-dimensional (3D) Dirac cones. This way, Cd$_3$As$_2$ would fit into an emergent class of materials which are nowadays referred to as 3D Dirac semimetals (for review see, e.g., Ref. [18]). These systems host 3D massless electrons described by the Dirac equation for particles with a vanishing rest mass, thus implying a conical band twice degenerated due to spin. The possible lack of inversion symmetry may lift this degeneracy and transform Cd$_3$As$_2$ into a 3D Weyl semimetal, with two pairs of Weyl cones. The lack or presence of inversion symmetry in Cd$_3$As$_2$ is still not resolved [19–21].

The theoretical prediction by Wang *et al.* [17] can be illustrated using a simple, currently widely accepted cartoonlike picture depicted in Fig. 2. It shows two 3D Dirac nodes, the points where the conical conduction and valence bands meet, located at the tetragonal $z$ axis of the crystal. Their protection is ensured by $C_4$ rotational symmetry [22]. With either increasing or decreasing energy, these two Dirac cones approach each other and merge into a single electronic band centered around the $\Gamma$ point, passing through a saddlelike Lifshitz point.
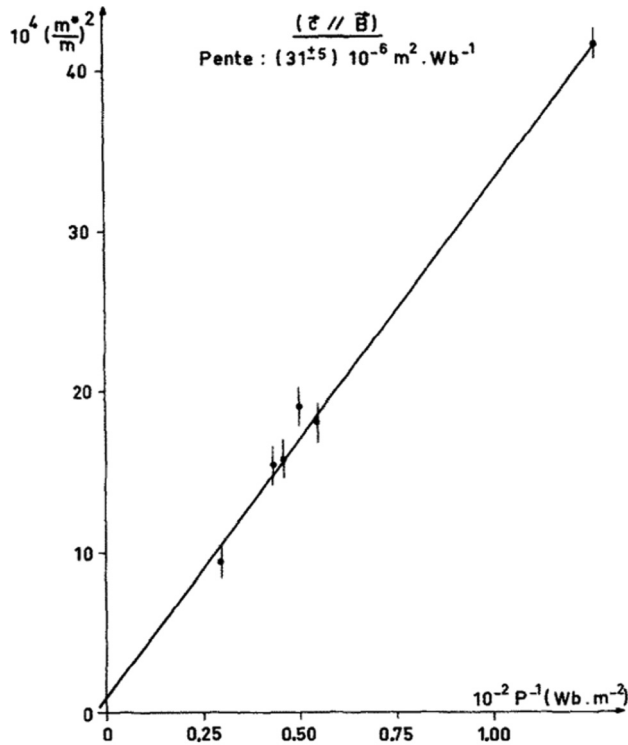
*milan.orlita@lncmi.cnrs.fr

FIG. 1. One of the very first experimental indications of a conical band in $Cd_3As_2$ presented by Rosenman [5]: the square of the cyclotron mass $m^*$, determined from the thermal damping of Shubnikov–de Haas oscillations, as a function of their inverse oscillation period $1/P$. The theoretically expected dependence for a conical band $m^2 = 2e\hbar/(Pv^2)$ allows us to estimate the velocity parameter $v = (1.1 \pm 0.1) \times 10^6$ m/s from the slope indicated in the plot. Reprinted from [5] with permission by Elsevier, copyright (1969).

The prediction of a 3D Dirac semimetallic phase in a material, which is not only well known in solid-state physics but also relatively stable under ambient conditions, stimulated a considerable experimental effort. The first angular-resolved photoemission spectroscopy (ARPES) and scanning tunneling microscopy/spectroscopy (STM/STS) experiments [23–26] confirmed the presence of widely extending conical features in the band structure, creating a large wave of interest. This wave gave rise to a number of experimental and theoretical studies, complementing those performed in the past, forming a rich knowledge of this material. As a result, cadmium arsenide now is among the most explored materials in current solid-state physics.

In addition to the extraordinarily high electronic mobility, cadmium arsenide exhibits a very strong linear magnetoresistance [6], an anomalous Nernst effect [27], and quantum Hall effect signatures when thinned down [28,29]. Furthermore, indications of the chiral anomaly, planar Hall effect, and electron transport through surface states have been reported [30–33]. Currently, these effects are all considered to be at least indirectly related to the specific relativisticlike band structure of this material. Yet surprisingly, consensus about the complex electronic band structure of $Cd_3As_2$ has not yet been fully established.
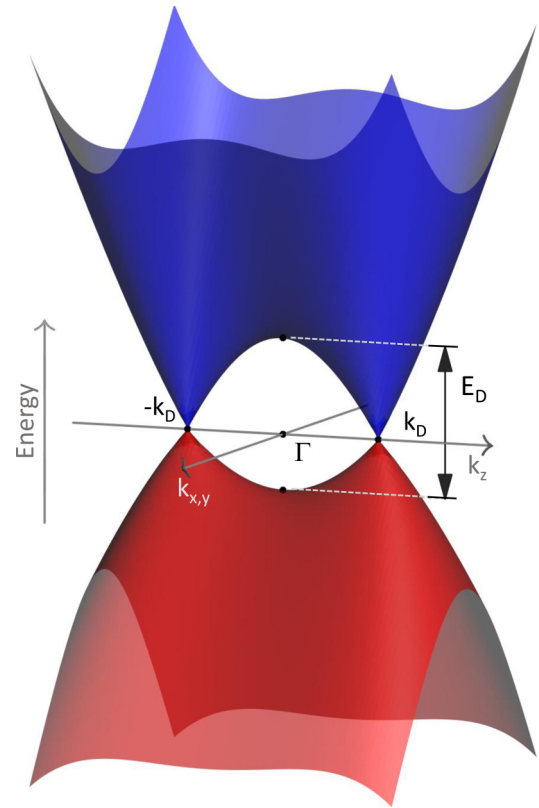


FIG. 2. A schematic view of the 3D Dirac cones in $Cd_3As_2$. Two symmetry-protected cones emerge in the vicinity of the $\Gamma$ point with the apexes located at the momenta $k = \pm k_D$ along the tetragonal axis of $Cd_3As_2$ (often associated with the $z$ axis). In general, the Dirac conical bands are characterized by an anisotropic velocity parameter ($v_x = v_y \neq v_z$) and possibly also by an electron-hole asymmetry. The energy scale of these cones (its upper bound) is given by the $E_D$ parameter, which refers to the energy distance between the upper and lower Lifshitz points.

A detailed understanding of the basic material parameters of $Cd_3As_2$ became essential for the correct interpretation of a wide range of observed, and yet to be discovered, physical phenomena. In this paper, we review the current knowledge of $Cd_3As_2$. We start with the properties of the crystal lattice and continue with the technological aspects of $Cd_3As_2$ growth. This is followed by a discussion of the theoretical and experimental investigation results, providing different possible views of this material's electronic bands. In particular, we focus on Dirac-type nodes, the most relevant aspect of the band structure when taking into consideration recent developments in this material's field.

## II. CRYSTAL LATTICE

Cadmium arsenide has a relatively complex crystal structure, with 160 atoms in the unit cell. It has been the subject of several x-ray studies, resulting in somewhat contradicting conclusions [1,19,20,34]. The current consensus implies that, at room and lower temperatures, which are the most relevant ones for fundamental and applied research conducted on this material, $Cd_3As_2$ is a tetragonal material with a unit cell of $a = b \approx 1.26$ nm and $c \approx 2.54$ nm. The particular space
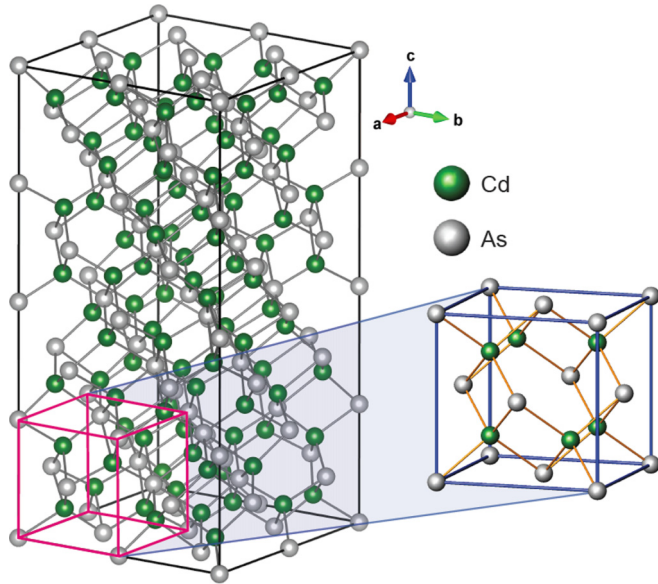
FIG. 3. The nonprimitive tetragonal unit cell of $Cd_3As_2$ is composed of $2\times2\times4$ weakly distorted antiflourite cells with two cadmium vacancies. This cell hosts 96 cadmium atoms and 64 arsenic atoms.

group remains a subject of discussion. More recent investigations favor a centrosymmetric group $I4_1/acd$ (No. 142) [20,34] over a noncentrosymmetric space group $I4_1cd$ (No. 110), as previously suggested [19]. The correct space-group assignment is of considerable importance for the complete understanding of $Cd_3As_2$. When space inversion symmetry is not present, spin degeneracy is lifted, and the Dirac nodes possibly split into pairs of Weyl nodes.

It is also important to note that the $Cd_3As_2$ crystal lattice, though clearly tetragonal, remains nearly cubic ($2a = 2b \approx c$) [20]. The lattice may therefore be seen, in the simplest approach, as being composed of antifluorite (cubic) cells with two missing cadmium cations (Fig. 3). Due to the cadmium vacancy ordering, a very large unit cell of $Cd_3As_2$ is formed. Composed of $2\times2\times4$ of antifluorite cells, it is oriented along the tetragonal $c$ axis, and contains 160 atoms (96 cadmium and 64 arsenic). Additionally, each single antifluorite cell is tetragonally distorted, with a small elongation along the $c$ axis ($c/2a \approx 1.006$) [20,35]. This simplified image of nearly cubic antifluourite cells, serving as building blocks for the entire $Cd_3As_2$ lattice, appears as a useful starting point for simplified effective models and *ab initio* calculations. Both are briefly discussed below. Finally, let us mention that above room temperature the crystal lattice of $Cd_3As_2$ undergoes a sequence of polymorphic phase transitions. The corresponding space group remains tetragonal but changes to $P4_2/nbc$ (No. 133) around $220\,^\circ$C and to $P4_2/nmc$ (No. 137) around $470\,^\circ$C [34,35]. At temperatures above $600\,^\circ$C, the symmetry of the crystal changes to a cubic one, characterized by the space group $Fm\bar{3}m$ (No. 225) [20]. Each of these phase transitions is accompanied by an abrupt change in lattice constants, leading to potential microcracks in the crystal. Notably, crystals of $Cd_3As_2$ can only be grown at temperatures above $425\,^\circ$C, regardless of the growth method.

The complexity of the crystal lattice directly impacts the physical properties of $Cd_3As_2$, as well as how we understand them. For instance, the large number of unit-cell atoms may partly complicate *ab initio* calculations of the electronic band structure. The complex crystal lattice, with a number of cadmium vacancies, may also be susceptible to small changes in ordering, possibly impacting distinct details in the electronic band structure. Some of the existing controversies about the electronic bands in $Cd_3As_2$ may thus stem from differences in the investigated samples' crystal structure, currently prepared using a wide range of crystal growth methods. The crystal-lattice complexity is also directly reflected in the optical response of $Cd_3As_2$, characterized by a large number of infrared and Raman-active phonon modes [36–38].

## III. TECHNOLOGY OF SAMPLE GROWTH

The technology of $Cd_3As_2$ growth encompasses a broad range of methods dating back over 50 years. These provide us with a multiplicity of sample forms: bulk or needlelike crystals, thin films, microplatelets, and nanowires. Not only monocrystalline or polycrystalline samples exist, but also amorphous [2] samples, all exhibiting different quality and doping levels. In the past, various techniques have been used, such as the Bridgman [13] and Czochralski [39,40] methods, sublimation in vacuum or in a specific atmosphere [41,42], pulsed-laser deposition [43], and directional crystallization in a thermal gradient [3]. The results of these techniques were summarized in review articles dedicated to the growth of $II_3V_2$ materials [35,44].

Most recently, the fast-developing field of $Cd_3As_2$ has been largely dominated by experiments [6,24–27,31,45] performed on samples prepared by either growth from a Cd-rich melt [20], or self-selecting vapor growth (SSVG) [46], which are described in the following in greater detail. With Cd-rich melt, $Cd_3As_2$ is synthesized from a Cd-rich mixture of elements sealed in an evacuated quartz ampoule, heated to $825\,^\circ$C, and kept there for 48 h. After cooling to $425\,^\circ$C at a rate of $6\,^\circ$C/h, $Cd_3As_2$ single crystals with a characteristic pseudohexagonal (112)-oriented facets are centrifuged from the flux.

The SSVG method comprises several steps [46]. In the first, the compound is synthesized from a stoichiometric mixture of elements in an evacuated sealed ampoule, and heated for 4 h $50\,^\circ$C above the $Cd_3As_2$ melting point. The resulting ingot is then purified using a sublimation process in an evacuated closed tube (kept around $800\,^\circ$C), refined with small amounts of excess metal or chalcogen elements (also at $50\,^\circ$C above the melting point), water quenched, annealed (around $700\,^\circ$C), and subsequently air cooled. Afterwards, the ingot is crushed and then sieved (targeting a particle size of 0.1–0.3 mm), with the obtained precursors then sealed in an evacuated ampoule. This is then inserted for about 10 days into a horizontal alumina furnace, whose temperature profile is shown in Fig. 4. The resulting crystals are plate-like or needlelike monocrystals, or polycrystals with large grains. The crystals have primarily (112)-oriented but occasionally also ($n$00)-oriented facets, with $n$ an even number (see Fig. 5).
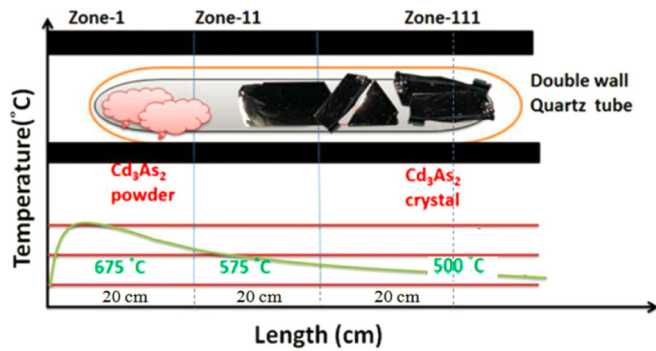
FIG. 4. Schematic cross-sectional side view of an alumina furnace used for self-selecting vapor growth of a $Cd_3As_2$ single crystal [46]. The positions of the ampoule in which transport takes place and the temperature profile of the furnace for $Cd_3As_2$ growth are shown. Reprinted from [46].

Crystals prepared using the two methods discussed above, as well as past methods, display $n$-type conductivity with a relatively high density of electrons. As-grown and without specific doping, the crystals rarely show an electron density below $10^{18}$ cm$^{-3}$. This translates into typical Fermi levels in the range of $E_F = 100$–$200$ meV measured from the charge-neutrality point. In literature this rather high doping is usually associated with the presence of arsenic vacancies [49]. The doping of $Cd_3As_2$ has been reported to vary with conventional annealing [50]. It seems to decrease after thermal cycling between room and helium temperatures [51]. A combined optical and transport study also revealed a relatively thick (10–20 $\mu$m) depleted layer on the surface of $Cd_3As_2$ crystals [52]. Optical studies also show relatively large inhomogeneities of up to 30% in the electron density, at the scale of hundred microns, in crystals prepared using different growth methods, with x-ray studies indicating the presence of systematic twinning [51].

Recently, there has been progress in other growth methods. These include the chemical vapor deposition (CVD) technique, employed to fabricate $Cd_3As_2$ nanowires [53]. Other methods, such as pulsed laser deposition in combination with solid phase epitaxy [28] and molecular beam epitaxy [29,54], have been successfully employed to prepare $Cd_3As_2$ layers with a thickness down to the nanometer scale. Most importantly, when the thickness of $Cd_3As_2$ films is reduced down to the tens of nanometers, ambipolar gating of $Cd_3As_2$ becomes possible [55].
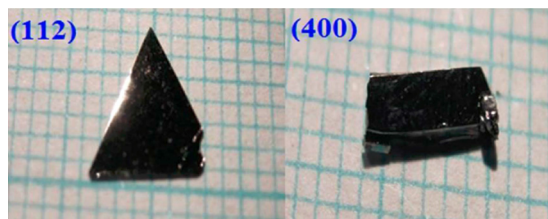


FIG. 5. $Cd_3As_2$ single crystals grown by the SSVG method. The larger facets are (112) and (even 00) planes, reaching an area up to 0.7 cm$^2$. Reprinted from [46].

## IV. ELECTRONIC BAND STRUCTURE: THEORETICAL VIEWS

Soon after the first experimental studies appeared [3,5,41,56,57], the band structure of $Cd_3As_2$ was approached theoretically. In this early phase, the electronic band structure was described using simple effective models, developed in the framework of the standard $k \cdot p$ theory. Such models were driven by the similarity between the crystal lattice, and presumably also electronic states, in $Cd_3As_2$, and conventional binary semiconductors/semimetals such as GaAs, HgTe, CdTe, or InAs [48]. In all of these materials, the electronic bands in the vicinity to the Fermi energy are overwhelmingly composed of cation $s$ states and anion $p$ states. In the case of $Cd_3As_2$, those are cadmiumlike cations and arseniclike anions.

In the first approach, the electronic band structure of $Cd_3As_2$ has been described using the conventional Kane model [58], which is widely applied in the field of zinc-blende semiconductors and which has also been successfully expanded to account for effects due to quantizing magnetic fields [59,60]. To the best of our knowledge, the very first attempt to interpret the experimental data collected on $Cd_3As_2$ using the Kane model was presented by Armitage and Goldsmid [12] in 1968. Later on, similar studies appeared [13,14,61,62] but with no clear consensus on the particular band structure parameters.

The size and nature of the band gap, describing the separation between the $p$-like and $s$-like states at the $\Gamma$ point, remained a main source of controversy [2]. Most often, relatively small values of either inverted or noninverted gaps have been reported, based on the analysis of different sets of experimental data [5,12,14]. Notably, when the band gap is significantly smaller than the overall energy scale of the considered band structure, the Kane model implies approximately conical conduction and valence bands, additionally crossed at the apex by a relatively flat band (Fig. 6) [63,64]. This band is usually referred to as being heavy-hole-like in semiconductor physics, and may be considered as flat only in the vicinity of the $\Gamma$ point. At larger momenta, it disperses with a characteristic effective mass close to unity.

Importantly, the presence of a 3D conical band in the Kane model is a result of an approximate accidental degeneracy of $p$-like and $s$-like states at the $\Gamma$ point, therefore making this cone not protected by any symmetry. Additionally, this cone is described by the Kane Hamiltonian [63], which is clearly different from the Dirac Hamiltonian. It should therefore not be confused with 3D Dirac cones subsequently predicted for $Cd_3As_2$ [17]. The term *massless Kane electron* was recently introduced [45,64–66] to distinguish those two types of 3D massless charge carriers. Therefore, at the level of the strongly simplifying Kane model, $Cd_3As_2$ does not host any massless 3D Dirac electrons. A nearly conical band, the presence of which was deduced from early transport experiments indicating energy-dependent effective mass [5,12] (Fig. 1), was then interpreted in terms of the Kane model assuming a nearly vanishing band gap.

An improved effective model, which takes into account the tetragonal nature of $Cd_3As_2$, not included in the conventional Kane model for zinc-blende semiconductors, has been
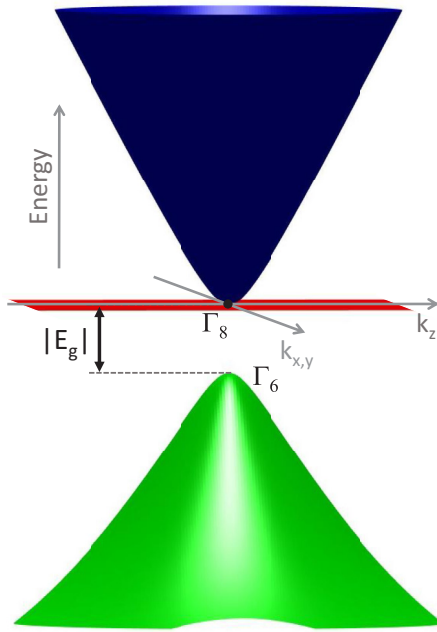
FIG. 6. The electronic band structure of a cubic semiconductor/semimetal implied by the Kane mode in the vicinity of the Brillouin zone center. At energies significantly larger than the band gap, both conduction and valence bands exhibit nearly conical shapes. For a negative band gap $E_g$ (chosen in the plotted case), the system is characterized by an inverted ordering of bands, and closely resembles the well-known semimetal HgTe [47]. A positive band gap would imply a band structure typical of narrow-gap semiconductors such as InSb [48].



FIG. 7. The schematic view of the electronic band structure of $Cd_3As_2$ proposed by Bodnar in Ref. [15]. Three electronic bands form two types of 3D conical structures: a single cone hosting Kane electrons at the large energy scale, appearing due to the vanishing band gap, and two highly tilted and anisotropic 3D Dirac cones at low energies. These are marked by vertical gray arrows and emerge due to the partly avoided crossing of the flat band with the conduction band. The energy scale of massless Dirac electrons $E_D$ exactly matches the size of crystal-field splitting parameter $\delta$.

proposed by Bodnar [15]. The tetragonal distortion of a nearly cubic lattice lifts the degeneracy of $p$-type states (light- and heavy-hole bands) at the $\Gamma$ point; this degeneracy is typical of all zinc-blende semiconductors [48]. A closer inspection of the theoretical band structure reveals two specific points at the tetragonal axis. At these points, the conduction and flat heavy-hole valence bands meet and form two highly anisotropic and tilted cones (Fig. 7). These may be associated with symmetry-protected 3D Dirac cones. Nevertheless, it was not until the work by Wang *et al.* [17] that such a prediction appeared explicitly in the literature. The crystal-field splitting parameter $\delta$ [68] is employed by Bodnar [15] to quantify the impact of the tetragonal distortion of the cubic lattice. This parameter directly corresponds to the energy scale $E_D$ of the symmetry-protected massless Dirac electrons in $Cd_3As_2$ (cf. Figs. 2 and 7). The work of Bodnar also inspired other theorists, who used the proposed model for electronic band structure calculations in quantizing magnetic fields [69–71].

The above-described effective models have been applied with some success to explain experimental data available those times. However, these models should be confronted with the much broader experimental knowledge acquired recently. Similar to all other models based on the $k \cdot p$ expansion, their validity is limited to the near vicinity of the Brillouin zone center, and to the number of spin-degenerate bands taken into account (restricted to 4 in the Kane/Bodnar model). Moreover, the number of band structure parameters is strongly restricted in these models. This ensures the models' relative simplicity,
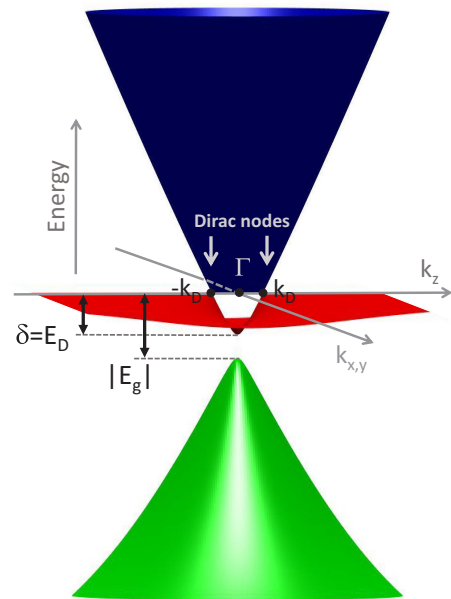
but at the same time, limits the potential to describe the band structure in greater detail, even in the immediate vicinity of the $\Gamma$ point.

It is therefore important to reconcile the implications of such effective models with other theoretical approaches. Such band structure calculations already appeared in the early stages of research on $Cd_3As_2$. These were based on either pseudopotential calculations [72–74] or the semiempirical tight-binding method [75]. More recently, *ab initio* calculations have been performed, with their main focus on the Dirac-like states. To the best of our knowledge, the first *ab initio* study of $Cd_3As_2$ predicting the presence of 3D massless Dirac electrons was presented by Wang *et al.* [17]. Nevertheless, the considered space groups did not comprise the most probable one, $I4_1/acd$ (No. 110) [20,34]. Other *ab initio* calculations may be found in Refs. [23,25,26,67,76], often carried out in support of experimental findings.

Even though the results of *ab initio* calculations may differ in some details, most likely related to the particular approximation of exchange and correlation functionals and the size of the unit cell considered, they provide us with a rather consistent theoretical picture of the electronic bands in $Cd_3As_2$. They predict that $Cd_3As_2$ is a semimetal, with a pair of well-defined 3D Dirac cones, emerging at relatively low energies. In line with symmetry arguments, the Dirac nodes are found to be located at the tetragonal axis, with an exception of Ref. [23].

When the noncentrosymmetric $I4_1cd$ space group is considered, the double degeneracy of the Dirac cones due to
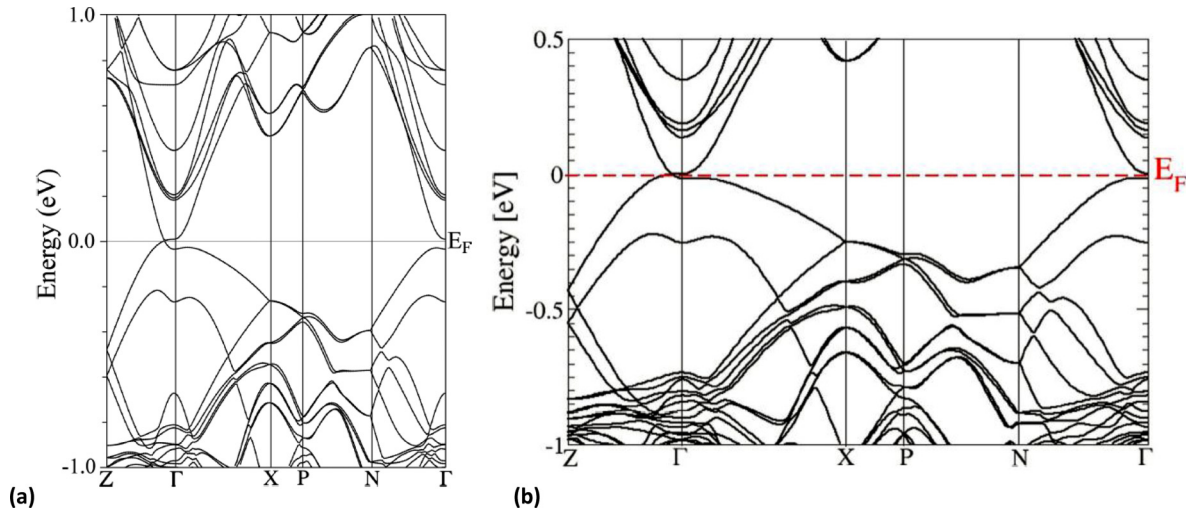
FIG. 8. The band structure of $Cd_3As_2$ deduced theoretically using *ab initio* approach by Ali *et al.* [20] and Conte *et al.* [67], using GGA approximations, in parts (a) and (b), respectively. In both cases, the 3D Dirac cones appear at the Fermi energy in close vicinity to the $\Gamma$ point, due the symmetry-allowed crossing of bands along the $\Gamma$-$Z$ line. The energy scale of the massless Dirac electrons $E_D$ in these two cases may be estimated to be 45 and 20 meV, respectively. Part (a) reprinted with permission from [20], copyright (2014) American Chemical Society. Part (b) reprinted from [67].

spin may be lifted [17]. The loss of inversion symmetry then transforms the 3D Dirac semimetal into a 3D Weyl semimetal with two pairs of Weyl nodes. The Dirac cones are dominantly formed from *p*-type arsenic states, and are well separated from the bands lying at higher or lower energies. Notably, the *s*-like cadmium states are found well below the Fermi energy. The band structure is therefore inverted and may be formally described by a negative band gap ($E_g \approx -0.5$ eV). To certain extent, the electronic bands in $Cd_3As_2$ resemble those in HgTe, which is another semimetal with an inverted band structure [47].

To illustrate the typical results of *ab initio* calculations, two examples have been selected from Refs. [20,67] and plotted in Figs. 8(a) and 8(b), respectively. The 3D Dirac cones are located in close vicinity to the $\Gamma$ point, with the charge neutrality (Dirac) points at the $\Gamma$-$Z$ line and the Fermi level.

The parameters of these cones derived in selected *ab initio* studies are presented in Table I. For instance, Conte *et al.* [67] deduced, using the generalized gradient approximation (GGA), that the energy scale of massless Dirac electrons reaches $E_D \approx 20$ meV, the strongly anisotropic velocity parameter is of the order of $10^5$ m/s, and two Dirac nodes are located at $k_D = \pm 0.23$ nm$^{-1}$.

Let us now explore the experiments carried out on $Cd_3As_2$ using various techniques. These provided us with unambiguous evidence for the conical features in this material. However, let us clearly note from the beginning that the scale of the conical bands deduced, using ARPES [23,25,26] and STM/STS [24] techniques, or from the optical response [20,37,45], is not consistent with the energy scale predictions for massless Dirac electrons based on *ab initio* calculations. While the theoretically expected scale of massless Dirac

TABLE I. The band structure parameters of $Cd_3As_2$: the energy scale $E_D$ (defined in Fig. 2), the Dirac point position $k_D$, and the crystallographic axis at which the Dirac nodes are located, as deduced using different experimental techniques or theoretical calculations/analysis. The velocity parameter is usually found to be around, or slightly below, $10^6$ m/s in the direction perpendicular to the line connecting Dirac nodes, and reduced down to the $10^5$ m/s range along this direction.

| Technique | Scale $E_D$ (meV) | Location $k_D$ (nm$^{-1}$) | Orientation |
|---|---|---|---|
| *ab initio*, GGA, $I4_1cd$ [17] | 40 | 0.32 | [001] |
| *ab initio*, GGA, $I4_1/acd$ [20] | 45 | 0.4 | [001] |
| *ab initio*, GGA, $I4_1/acd$ [67] | 20 | 0.23 | [001] |
| *ab initio*, GGA, $I4_1cd$ [23] | 200 | 1.2 | [112][a] |
| ARPES [23] | several hundred | 1.6 | [112][a] |
| ARPES [26] | several hundred | | [001] |
| ARPES [25] | several hundred | | [001] |
| STM/STS [24] | 20 | 0.04 | [001] |
| Magneto-optics [45,77] | <40 | <0.05 | [001] |
| Magnetotransport and Bodnar model [5,15] | 85 | 0.15 | [001] |
| Magnetotransport [78] | <200 | | [001] |

[a]Equivalent to the [111] direction when the cubic cell approximation is considered as in Ref. [23].
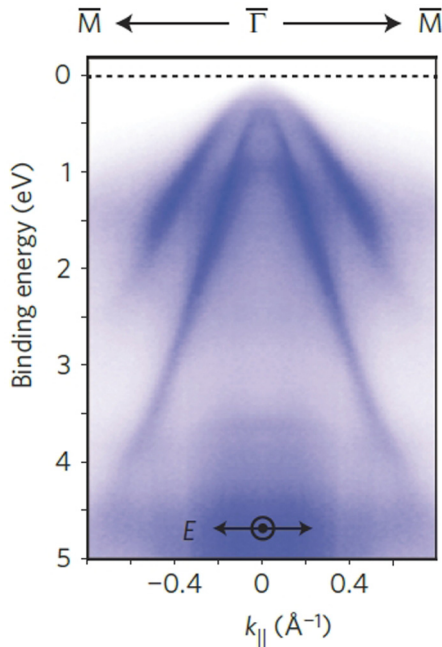
FIG. 9. The valence bands in $Cd_3As_2$ visualized by low-temperature ARPES technique by Liu *et al.* [23]. The data were collected on the (112)-terminated surface. The widely extending 3D conical band, characterized by a velocity parameter of $1.3 \times 10^6$ m/s and interpreted in terms of 3D massless Dirac electrons, coexists with another holelike weakly dispersing parabolic band, also observed in Ref. [26]. Reprinted by permission from Springer Nature: Nature Materials [23], copyright (2014).

electrons rarely exceeds $E_D \sim 100$ meV (Table I), the experimentally observed cones extend over a significantly broader interval of energies.

In the following sections, we employ, for the sake of brevity, a simplified notation and refer to the Kane and Dirac models, which both may, at least from the theoretical viewpoint, explain the presence of massless electrons in $Cd_3As_2$. In the case of the Dirac model, we always consider 3D massless electrons, which are described by the Dirac equation with the zero rest mass and the presence of which is protected by the discrete $(C_4)$ rotational symmetry [17]. In the case of Kane model, zero or vanishing band gap is implicitly assumed.

## V. ANGULAR-RESOLVED PHOTOEMISSION SPECTROSCOPY

The ARPES technique provided us with a solid piece of evidence for conical features in the electronic band structure of $Cd_3As_2$, soon after predictions of Dirac-type states by Wang *et al.* [17]. This largely contributed to the renewed interest in the electronic properties of this material. Such initial observations were made by several groups [23,25,26,79], and elaborated further later on [80].

Characteristic data collected in ARPES experiments on $Cd_3As_2$ [23,26] are plotted in Figs. 9 and 10, and respectively show well-defined conical features for both valence and conduction bands. The conical features in Figs. 9 and 10 were interpreted in terms of bulk states. Liu *et al.* [23] and Neupane *et al.* [26] concluded the presence of a pair
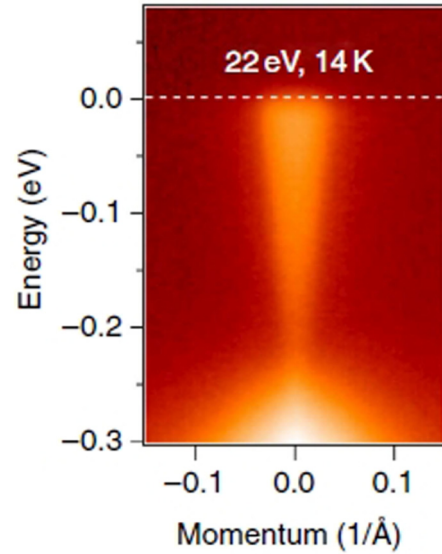


FIG. 10. The conduction band of $Cd_3As_2$ visualized by ARPES by Neupane *et al.* [26]. The data were collected on the (001)-terminated surface of $Cd_3As_2$ at 14 K and show the dispersion in the direction perpendicular to the $\Gamma$-$Z$ line. The observed 3D conical band was interpreted in terms of 3D massless Dirac electrons, implying a velocity parameter of $1.5 \times 10^6$ m/s. Reprinted by permission from Springer Nature: Nature Communications [26], copyright (2014).

of 3D Dirac nodes at the [112] and [001] axes, respectively. However, it is worth noting that the orientation along the [112] axis or, alternatively, along the [111] axis when an approximately cubic unit cell is considered like it is the case in Ref. [23], is not consistent with expectations based on symmetry arguments [22], which only allow the Dirac nodes to be present at the tetragonal axis (the [001] direction). The velocity parameter was found to be close to $10^6$ m/s in the plane perpendicular to the axis connecting the Dirac nodes, and reduced down to $3 \times 10^5$ m/s [23] along this axis. The ARPES data in Refs. [23,26] do not directly show any signatures of Dirac cones merging via the corresponding Lifshitz points. Nevertheless, the indicated velocity parameters, and the position of the cones $(k_D)$, allow us to estimate the scale of massless Dirac electrons $E_D$ to be several hundred meV or more.

ARPES data similar to Refs. [23,26], obtained on the [112]-terminated surface of $Cd_3As_2$, were also presented by Borisenko *et al.* [25], who primarily focused on the conical feature in the conduction band. The presence of a pair of symmetry-protected 3D Dirac cones, with the corresponding nodes at the [001] axis, has been concluded, and the electron velocity parameter $v \approx 0.8 \times 10^6$ m/s deduced. The Fermi energy in the studied $n$-doped sample exceeded $E_F \approx 200$ meV, and may serve as a lower bound for the $E_D$ parameter. Since the shape of the observed conical band does not provide any signature of the approaching upper Lifshitz point, one may conclude that $E_D \gg E_F$.

The basic parameters of Dirac-type conical bands deduced from the above-cited ARPES experiments have been compared in Table I with results of other experimental techniques,

which are discussed in detail later on. One may see that there is a considerable spread of the reported values for both the energy scale and the position of the Dirac cones in $Cd_3As_2$. For instance, the energy scale consistent with the ARPES data exceeds by almost two orders of magnitude the estimate based on STM/STS measurements [24]. At present, the reason for this disagreement remains unclear.

More recently, other ARPES experiments on $Cd_3As_2$ have been performed by Roth *et al.* [80]. They provided experimental data similar to previous studies, but differed in their interpretation. From their experiment realized on a sample with a (112)-terminated surface, they concluded that a part of observed conical features does not come from bulk, but instead originates from the surface states (cf. Ref. [79]). Let us note that, since each Dirac node is composed of two Weyl nodes with opposite chiralities [81], such surface states may have the form of the Fermi arcs in a 3D symmetry-protected Dirac semimetal.

To the best of our knowledge, the electronic band structure observed in ARPES experiments has not yet been in detail compared with expectations of the Kane/Bodnar model. Nevertheless, it is interesting to note that the conical valence band observed in the ARPES data (Fig. 9) coexists with another weakly dispersing holelike parabolic band [26], which has a characteristic effective mass close to unity. Such a band is not expected in the model of 3D massless Dirac electrons, nevertheless, it could be straightforwardly explained within the Kane/Bodnar picture with a small or vanishing band gap.

## VI. SCANNING TUNNELING SPECTROSCOPY AND MICROSCOPY

Similar to ARPES, the STS/STM technique also played an important role in the recent revival of $Cd_3As_2$. The data collected in STS experiments performed in magnetic fields [24] revealed, via the characteristic $\sqrt{B}$ dependence of Landau levels, the presence of a single widely extending conical band located at the center of the Brillouin zone (see Fig. 11). In the literature, this observation is often taken as experimental evidence for the symmetry-protected 3D massless Dirac electrons in $Cd_3As_2$. However, according to Jeon *et al.* [24], the existence of "this extended linearity is not guaranteed by the Dirac physics around the band inversion."

Such a conclusion agrees with theoretical expectations based on symmetry arguments. These exclude the existence of a symmetry-protected Dirac cone located at the center of the Brillouin zone [22]. In addition, this observation is in line with the Kane/Bodnar models used to explain the band structure of $Cd_3As_2$ in the past. Nevertheless, Jeon *et al.* [24] also conclude, by extrapolating their Landau-level spectroscopy data to vanishing magnetic fields, that a pair of symmetry-protected Dirac cones emerges at low energies. They give a rough estimate of $E_D \approx 20$ meV for the characteristic Dirac energy scale.

Beyond insights into the bulk electronic states of $Cd_3As_2$, the natural sensitivity of the STM/STS technique to the surface of explored systems may provide us with deeper knowledge about their surface states. A 3D symmetry-protected Dirac semimetal like $Cd_3As_2$ can be viewed as two copies of a 3D Weyl semimetal with nodes having opposite chi-
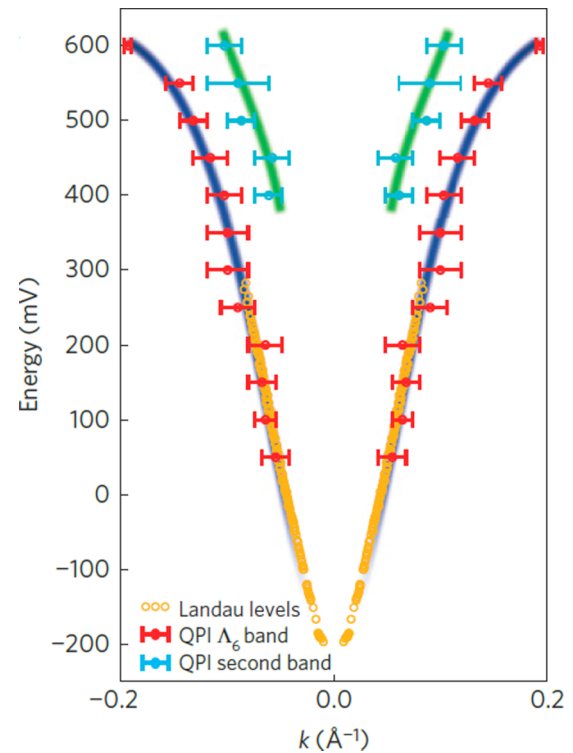


FIG. 11. The approximately conical band centered at the $\Gamma$ point deduced from Landau-level spectroscopy (open circles) and quasiparticle interference (QPI) pattern (closed circles with error bars) in the STS/STM experiments performed by Jeon *et al.* [24]. The slope of the conical band corresponds to a velocity parameter of $0.94 \times 10^6$ m/s. Reprinted by permission from Springer Nature: Nature Materials [24], copyright (2014).

ralities; two sets of Fermi arcs are expected on the surface (see Ref. [82] for details). The recent STS/STM study [83] dedicated to the surface reconstruction of cadmium vacancies in $Cd_3As_2$ may be considered as the initial step in such investigations.

## VII. OPTICAL PROPERTIES

The optical and magneto-optical properties of $Cd_3As_2$ have been a topic of study for more than 50 years, and resulted in a series of works [4,56,84]. These were often interpreted in terms of Kane/Bodnar models [13,38,45,51,61,70,77,85–91], and more recently using the picture of 3D massless Dirac electrons [37,54,92,93].

Early optical studies were focused on the basic character of the electronic band structure in $Cd_3As_2$. They aimed at clarifying the existence of a band gap and at determining its size. Using infrared reflectivity and transmission techniques, Turner *et al.* [4] concluded that $Cd_3As_2$ should be classified as a narrow-gap semiconductor with a direct band gap of 0.16 eV. Similarly, an indirect band gap around 0.2 eV, was concluded by Zdanowicz *et al.* [84] based on transmission experiments. Much lower values were found in magneto-optical studies. Haidemenakis *et al.* [56] concluded $E_g < 30$ meV, suggesting a semimetallic nature of $Cd_3As_2$. The difference

in conclusions between optical and magneto-optical studies may be related to the large doping of the explored samples. In that case, the onset of interband absorption, often referred to as the optical band gap, appears due to the Moss-Burstein shift (Pauli blocking) [94], at photon energies significantly exceeding the size of the energy band gap.

Further series of optical and magneto-optical $Cd_3As_2$ studies were performed on various monocrystalline or polycrystalline samples during the 1970's and 1980's. The collected data were primarily analyzed within the framework of the Kane model [13,61,85–87], and later on the Bodnar model [88,89,91]. The authors of these works concluded that the electronic band structure at the $\Gamma$ point is fairly well described using these models: it is inverted, with the $p$-type arsenic states above the $s$-like cadmium states, and characterized by a relatively small negative band gap. A schematic view of such a band structure is plotted in Figs. 6 and 7. The deduced value of the band gap reached $E_g \approx -0.2$ eV [61,85,86] at room or low temperatures, but also values as low as $E_g \approx -0.1$ eV have been reported [88,89,91]. Particular attention has been paid to the profile and position of the weakly dispersing band, which is nearly flat in the vicinity of the $\Gamma$ point. Several times, the possibility of the band maxima located at nonzero momenta has been discussed [61,87]. At the same time, Lamrani and Aubin concluded a surprisingly flat heavy-hole band, when the theoretically expected Landau-quantized Bodnar band structure [70,90] was confronted with the experimentally determined energies of interband inter-Landau-level excitations [91].

The renewed interest in $Cd_3As_2$ motivated several groups to take a fresh look at the optical, magneto-optical, and ultrafast optical properties of this material [37,45,51,54,77,92,95–99]. Thanks to this, the optical conductivity of $Cd_3As_2$ (Fig. 12) has been extracted from the experimental data [37]. At low energies, the optical conductivity is characterized by a pronounced Drude peak due to the presence of free charge carriers, and a rich set of phonon excitations. Similar to the Raman response [36,96], the complexity of the phonon-related response directly reflects the relatively high number of atoms in the $Cd_3As_2$ unit cell. Above the onset of interband absorption, optical conductivity increases with a slightly superlinear dependence on photon energy. Such behavior is not far from the expectation for 3D massless charge carriers $\sigma(\omega) \propto \omega$ [100,101]. The observed optical response was thus interpreted in terms of 3D massless Dirac electrons, with a low anisotropy and a velocity parameter lying in the range of $1.2$–$3.0 \times 10^5$ m/s. No clear indications of Dirac cones merging at the Lifshitz points were found. Reflectivity data similar to Ref. [37] were also presented by Jenkins *et al.* [92], with basically the same conclusions.

The Dirac model was similarly used to interpret the classical-to-quantum crossover of cyclotron resonance observed in magnetotransmission data collected on thin MBE-grown $Cd_3As_2$ layers [54] as well as pump-probe experiments in the visible spectral range, which revealed the transient reflection [95] and transmission [97]. These latter experiments show that a hot carrier distribution is obtained after 400–500 fs, after which the charge carriers relax by two processes. Subsequent pump-probe experiments using mid-infrared [98] and THz probe [99] confirm this two-process
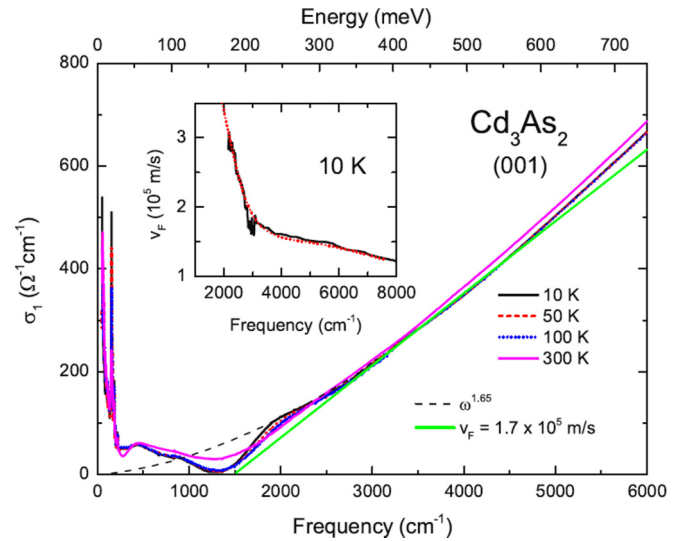


FIG. 12. The real part of the optical conductivity of $Cd_3As_2$ obtained by Neubauer *et al.* [37]. At low energies, the conductivity is dominated by Drude (free-carrier) response accompanied by a series of infrared-active phonon modes. Above the onset of the interband absorption around 1500–2000 cm$^{-1}$, the optical conductivity increases roughly linearly with the photon energy, which is behavior expected for massless charge carries in 3D. Reprinted with permission from [37], copyright (2016) by the American Physical Society.

relaxation, which can be qualitatively reproduced using a two-temperature model.

A different view was proposed in a recent magnetoreflectivity study of $Cd_3As_2$ by Akrap *et al.* [45] (see Fig. 13). In high magnetic fields, when the samples were pushed into their corresponding quantum limits with all electrons in the
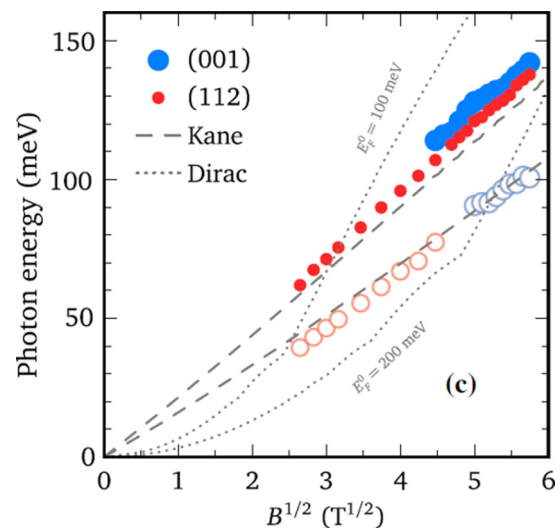


FIG. 13. The energies of cyclotron resonance excitations observed in Ref. [45] as a function of applied magnetic field, obtained on (112)- and (001)-oriented $Cd_3As_2$ samples. The dashed and dotted lines show theoretically expected positions within the Kane and Dirac models (see Ref. [45] for details). Adapted with permission from [45], copyright (2016) by the American Physical Society.

lowest Landau level, the $\sqrt{B}$ dependence of the observed cyclotron mode was found to be inconsistent with 3D massless Dirac electrons. The data were interpreted in terms of the Kane/Bodnar model, with a vanishing band gap. This model also leads to the appearance of 3D massless electrons and, consequently, to a magneto-optical response linear in $\sqrt{B}$. In this model, the $\sqrt{B}$ dependence of the cyclotron mode is also expected in the quantum limit. This is in contrast to 3D massless Dirac electrons, which host characteristic so-called zero-mode Landau levels. These are independent of magnetic field, disperse linearly with momentum along the direction of the applied field, and imply a more complex cyclotron resonance dependence in the quantum limit. An approximately isotropic velocity parameter was found for the nearly conical conduction band: $v \approx 0.9 \times 10^6$ m/s [45]. Estimates of the band gap and crystal-field splitting parameter at low temperatures were obtained in a subsequent magnetotransmission study performed on thin $Cd_3As_2$ slabs [77]: $E_g = -(70 \pm 20)$ meV and $|\delta| = E_D < 40$ meV.

Lately, spatially resolved infrared reflectivity has been used to characterize the homogeneity of $Cd_3As_2$ crystals [51]. In all the studied samples, independently of how they were prepared and how they were treated before the optical experiments, conspicuous fluctuations in the carrier density up to 30% have been found. These charge puddles have a characteristic scale of 100 $\mu$m. They become more pronounced at low temperatures and, possibly, they become enhanced by the presence of crystal twinning. Such an inhomogeneous distribution of electrons may be a generic property of all $Cd_3As_2$ crystals, and should be considered when interpreting experimental data collected using other techniques.

## VIII. MAGNETOTRANSPORT PROPERTIES AND QUANTUM OSCILLATIONS

Renewed interest in $Cd_3As_2$ brought upon an explosion of interest in magnetotransport studies. Many of these studies focused on the previously reported very high carrier mobility [3], and its possibilities for device application. Often, newer transport results are interpreted within the scenario of two 3D Dirac cones, which are well separated in $k$ space and with the Fermi level lying below the Lifshitz transition.

The first detailed magnetotransport study of $Cd_3As_2$ dates back to the 1960's [5,12,102]. The geometry of the Fermi surface was, to the best of our knowledge, for the first time addressed by Shubnikov–de Haas (SdH) measurements. Rosenman [102] explored such quantum oscillations on a series of $n$-doped samples, concluding that the Fermi surface is a simple ellipsoid symmetric around the $c$ axis, and inferred a low anisotropy factor of 1.2. These very first papers also show nearly conical shape of the conduction band (Fig. 1). A decade later, Zdanowicz et al. [103] studied SdH oscillations in thin films and single crystals of $Cd_3As_2$, confirming the ellipsoidal geometry of the Fermi surface. In addition, they reported a striking linear magnetoresistance (MR).

In a new bout of activity, several groups confirmed that the Fermi surface consists of a simple, nearly spherical ellipsoid, with an almost isotropic Fermi velocity [6]. Such a simple

Fermi surface was questioned by Zhao et al. [78]. They found that, for particular directions of the magnetic field with respect to the main crystal axes, the magnetoresistance (MR) shows two oscillation periods which mutually differ by 10%–25%, pointing to a dumbbell-shaped Fermi surface. This was interpreted to originate from two nested Fermi ellipsoids arising from two separated Dirac cones, where $E_F$ is placed just above the Lifshitz transition. Another picture was proposed by Narayanan et al. [104], who found single-frequency SdH oscillations, and concluded two nearly isotropic Dirac-type Fermi surfaces. In subsequent studies, Desrat et al. followed the SdH oscillations as a function of the field orientation, and always found two weakly separated frequencies (5%–10%). Their results were interpreted within the picture of two ellipsoids that are separated in $k$ space due to the possible absence of inversion symmetry [21]. Clear beating patterns, indicating a multiple frequency in SdH oscillations, were also reported in Nernst measurements [27] and magnetoresistance [105] on single crystals of $Cd_3As_2$. Such beating patterns were attributed to the lifting of spin degeneracy due to inversion symmetry breaking either by an intense magnetic field [27,106], or by Cd-antisite defects [105], which may turn a Dirac node into two Weyl nodes.

Several transport studies reported on strikingly linear non-saturating MR in $Cd_3As_2$ [6,104,107] being more pronounced in samples with lower mobilities. Since linear MR is observed at magnetic fields far below the quantum limit, the standard Abrikosov's theory [108], referring to the transport in the lowest Landau level, cannot be applied, and a different explanation was needed. Liang et al. [6] therefore suggest there is a mechanism that protects from backscattering in zero field. This protection is then rapidly removed in field, leading to a very large magnetoresistance. They propose an unconventional mechanism, caused by the Fermi surface splitting into two Weyl pockets in an applied magnetic field. Similarly, Feng et al. [107] assigned the large nonsaturating MR to a lifting of the protection against backscattering, caused by a field-induced change in the Fermi surface. The authors judged that linear MR cannot be due to disorder, as the $Cd_3As_2$ samples are high-quality single crystals. They instead conclude that it is due to the Dirac node splitting into two Weyl nodes. In contrast, Narayanan et al. [104] find that the Fermi surface does not significantly change up to 65 T, except for Zeeman splitting caused by a large $g$ factor. Through comparing quantum and transport relaxation times, they conclude that transport in $Cd_3As_2$ is dominated by small-angle scattering, which they trace back to electrons scattered on arsenic vacancies, and that the linear MR is linked to mobility fluctuations.

The Potter et al. theory [81] predicts the existence of specific closed cyclotron orbits in a Dirac or Weyl semimetal [Fig. 14(a)]. These orbits are composed of two Fermi arcs located on opposite surfaces of the sample, which are then interconnected via zero-mode Landau levels. Moll et al. [31] report on the SdH oscillations measured in mesoscopic devices. These were prepared using the focused ion beam technique, allowing $Cd_3As_2$ crystals to be cut into submicron-thick platelets. They report two series of oscillations, and via specific angle dependence, they associate them with surface-related and bulk-related orbits [Fig. 14(b)].
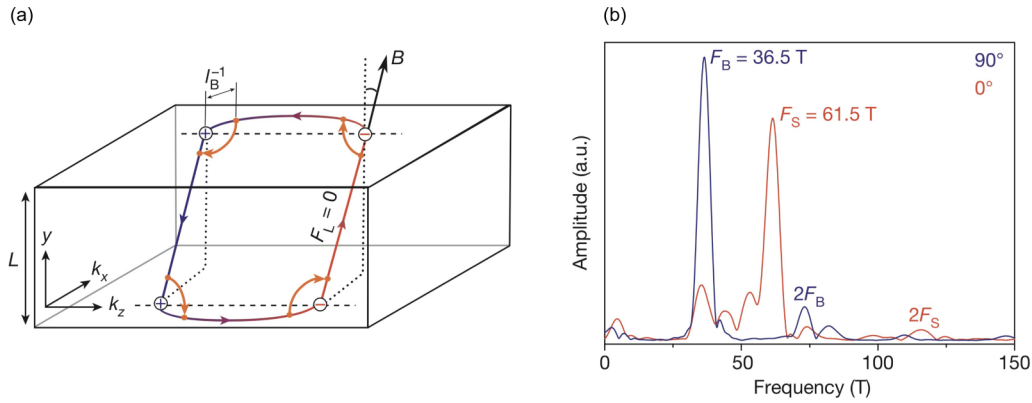
FIG. 14. (a) Weyl orbit in a thin slab of thickness $L$ in a magnetic field $B$. The orbit involves the Fermi-arc surface states connecting the Weyl nodes of opposite chirality, and the bulk states of fixed chirality. (b) The Fourier transform of magnetoresistance at $T = 2$ K measured on a thin $Cd_3As_2$ sample ($L = 150$ nm) which was cut from a single crystal by focused ion beam. The field was oriented parallel (90°) and perpendicular (0°) to the surface. Only one frequency is observed for parallel field, and two frequencies for perpendicular field. Adapted by permission from Springer Nature: Nature [31], copyright (2016).

The chiral anomaly is yet another theoretically expected signature of the field-induced splitting of a Dirac point into a pair of Weyl nodes. The parallel application of an electric and magnetic field is predicted to transfer electrons between nodes with opposite chiralities. Such a transfer should be associated with lowering resistivity (negative MR). For $Cd_3As_2$, there are indeed several reports of a negative MR and a suppression of thermopower for particular magnetic-field directions [30,32,109]. Typically, such behavior was observed in microdevices (platelets or ribbons). It should be noted that a negative MR can also emerge in a topologically trivial case due to so-called current jetting [110,111]. This is a simple consequence of a high transport anisotropy when a magnetic field is applied. In such a case, the current is jetting through a very narrow part of the sample. The measured MR then strongly depends on the distance of the voltage contacts from the current path.

The analysis of the quantum oscillation phase represents a unique way to identify the nature of probed charge carriers. For conventional Schrödinger electrons, one expects so-called Berry phase $\beta = 0$, whereas massless Dirac electrons should give rise to $\beta = \pi$. Indeed, several reports based on SdH oscillations in $Cd_3As_2$ indicate that $\beta \sim \pi$ [103,112–114]. A weak deviation from the ideal nontrivial Berry phase $\beta = (0.8–0.9)\pi$ was reported by Narayanan [104], who also discussed the influence of Zeeman splitting on the phase of quantum oscillations [115]. Notably, the electron $g$ factor in $Cd_3As_2$ is relatively large and anisotropic, and it implies Zeeman splitting comparable to the cyclotron energy [16,116].

Contrasting results were obtained by Xiang *et al.* [106], who found the nontrivial Berry phase only when the field is applied along the tetragonal $c$ axis of $Cd_3As_2$. When the magnetic field is rotated to be parallel with the $a$ or $b$ axis, the measured Berry phase becomes nearly trivial (see Fig. 15
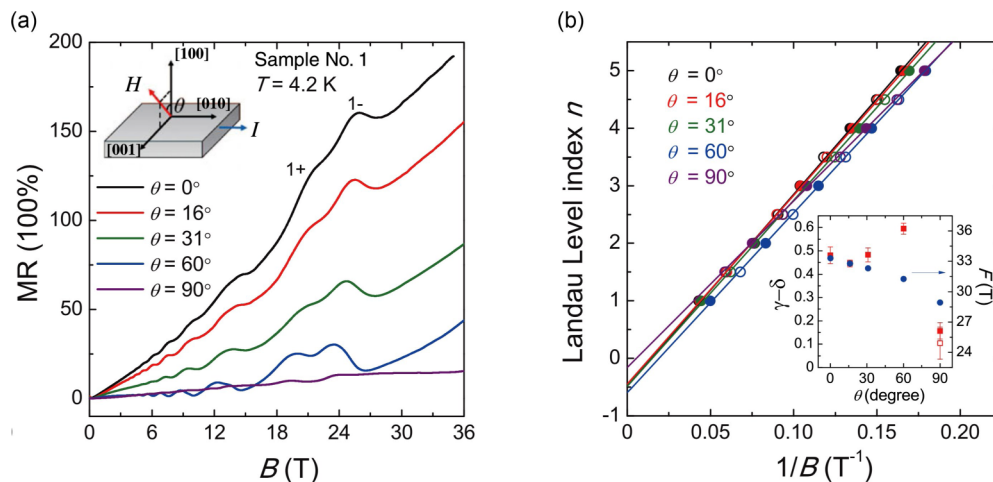


FIG. 15. (a) Angular dependence of the transverse magnetoresistance with magnetic field $B$ rotated in the (010) plane. The tilt angle $\theta$ is the angle between $B$ and the [100] direction. (b) Landau index plots $n$ vs $1/B$ at different $\theta$'s. (Inset) Angular dependence of the oscillation frequency $F$ and the total phase $\gamma - \delta$, extracted from the linear fitting from the first Landau level to the fifth Landau level. Adapted with permission from [106], copyright (2015) by the American Physical Society.
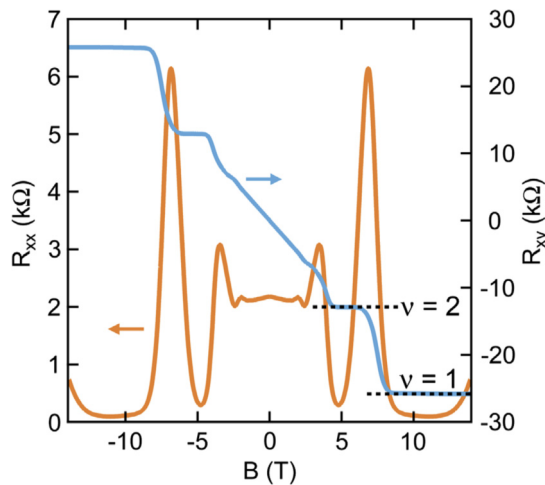
FIG. 16. The quantum Hall effect in a 20-nm-thick epitaxial $Cd_3As_2$ film grown by molecular beam epitaxy, showing the Hall ($R_{xy}$) and longitudinal ($R_{xx}$) resistances as a function of magnetic field measured at 1 K. Reprinted with permission from [29], copyright (2018) by the American Physical Society.

and discussion in Ref. [117]). This result is interpreted in terms of 3D Dirac-phase symmetry-breaking effects, when the magnetic field is tilted away from the $c$ axis. A certain angle dependence of the Berry phase has also been reported by Zhao *et al.* [78], reporting the Berry phase in-between 0 and $\pi$. Another study by Cheng *et al.* [118] was dedicated to the thickness dependence of the Berry phase in MBE-grown thin films of $Cd_3As_2$, implying a nontrivial to trivial transition of the Berry phase with changing the layer thickness.

The partly contradicting results in determining the Berry phase illustrate that even though the phase of quantum oscillation in principle identifies the nature unambiguously, the practical analysis of this phase is straightforward only in well-defined system such as graphene [119]. In more complex materials such as $Cd_3As_2$, where quantum oscillations are superimposed on the much stronger effect of linear magnetoresistance [6], the precise and reliable determination of the phase may represent a more challenging task. This may be illustrated with the example of bulk graphite, which is another high-mobility system with a strong and approximately linear magnetoresistance. There, the Dirac-type or normal massive nature of hole-type carriers has been a subject of intensive discussion in literature [120–124].

More recently, the very first experiments showing the quantum Hall effect (QHE) in thin films of $Cd_3As_2$ appeared. Zhang *et al.* measured SdH oscillations on a series of $Cd_3As_2$ nanoplates [125]. They report multiple cyclotron orbits, distinguishing both 3D and 2D Fermi surfaces. They also observe a quantized Hall effect (QHE), which they attribute to the

surface states of $Cd_3As_2$, linked to the Weyl orbits. Schumann *et al.* [29] studied MBE-grown, 20-nm-thick films of $Cd_3As_2$, and observed the QHE at low temperatures (Fig. 16). Similarly, they attribute the QHE to surface states, and conclude that the bulk states are weakly gapped at low temperatures. In continuation of this work, Galletti *et al.* [55] tuned the carrier concentration in thin films across the charge neutrality point using a gate voltage and concluded that the observed magnetotransport response is in line with expectations for a 2D electron gas of massless Dirac electrons.

The planar Hall effect has also been reported in $Cd_3As_2$, an effect in which a longitudinal current and an in-plane magnetic field give rise to a transverse current or voltage. Li *et al.* investigated microribbons of $Cd_3As_2$, and found an anisotropic MR and planar Hall effect, which they attribute to the physics of Berry curvature [126]. Guo *et al.* also uncovered unusually large transverse Hall currents in needlelike single crystals of $Cd_3As_2$ [105]. Wu *et al.* carried out similar measurements on $Cd_3As_2$ nanoplatelets, finding a large negative longitudinal MR, and a planar Hall effect with nonzero transverse voltage when the magnetic field is tilted away from the electric field. These observations are interpreted as transport evidence for the chiral anomaly [33].

## IX. SUMMARY

Cadmium arsenide is a prominent member of the topological materials class, widely explored using both theoretical and experimental methods. At present, there is no doubt that $Cd_3As_2$ hosts well-defined 3D massless charge carriers. These are often associated with the symmetry-protected 3D Dirac phase, but may also be interpreted using alternative approaches developed in the past. This calls for further investigations of $Cd_3As_2$, preferably using a combination of different experimental techniques. Such investigation may resolve the currently existing uncertainties about the electronic band structure, which slow down the overall progress in physics of $Cd_3As_2$, and may contribute to our understanding of rich phenomena associated with this appealing material.

[1] M. v. Stackelberg and R. Paulu, Z. Phys. Chem. B **28**, 427 (1935).

[2] W. Zdanowicz and L. Zdanowicz, Annu. Rev. Mater. Sci. **5**, 301 (1975).

[3] A. J. Rosenberg and T. C. Harman, J. Appl. Phys. **30**, 1621 (1959).

[4] W. J. Turner, A. S. Fischler, and W. E. Reese, Phys. Rev. **121**, 759 (1961).

[5] I. Rosenman, J. Phys. Chem. Solids **30**, 1385 (1969).

[6] T. Liang, Q. Gibson, M. N. Ali, M. Liu, R. Cava, and N. Ong, Nat. Mater. **14**, 280 (2015).

[7] J.-P. Michenaud and J.-P. Issi, J. Phys. C: Solid State Phys. **5**, 3061 (1972).

[8] N. B. Brandt, S. M. Chudinov, and Y. G. Ponomarev, *Modern Problems in Condensed Matter Sciences* (North-Holland, Amsterdam, 1988), Vol. 20.1.

[9] E. H. Hwang and S. Das Sarma, Phys. Rev. B **77**, 235437 (2008).

[10] K. I. Bolotin, K. J. Sikes, J. Hone, H. L. Stormer, and P. Kim, Phys. Rev. Lett. **101**, 096802 (2008).

[11] P. Neugebauer, M. Orlita, C. Faugeras, A.-L. Barra, and M. Potemski, Phys. Rev. Lett. **103**, 136403 (2009).

[12] D. Armitage and H. Goldsmid, Phys. Lett. A **28**, 149 (1968).

[13] L. M. Rogers, R. M. Jenkins, and A. J. Crocker, J. Phys. D: Appl. Phys. **4**, 793 (1971).

[14] L. G. Caron, J. P. Jay-Gerin, and M. J. Aubin, Phys. Rev. B **15**, 3879 (1977).

[15] J. Bodnar, in *Proceedings of the III Conference on Narrow-Gap Semiconductors, Warsaw*, edited by J. Raułuszkiewicz, M. Górska, and E. Kaczmarek (Elsevier, Amsterdam, 1977), p. 311; see also arXiv:1709.05845.

[16] F. Blom, in *Narrow Gap Semiconductors. Physics and Applications*, edited by W. Zawadzki, Lecture Notes in Physics Vol. 133 (Springer, Berlin, 1980).

[17] Z. Wang, H. Weng, Q. Wu, X. Dai, and Z. Fang, Phys. Rev. B **88**, 125427 (2013).

[18] N. P. Armitage, E. J. Mele, and A. Vishwanath, Rev. Mod. Phys. **90**, 015001 (2018).

[19] G. A. Steigmann and J. Goodyear, Acta Crystallogr. Sect. B **24**, 1062 (1968).

[20] M. N. Ali, Q. Gibson, S. Jeon, B. B. Zhou, A. Yazdani, and R. J. Cava, Inorg. Chem. **53**, 4062 (2014).

[21] W. Desrat, S. S. Krishtopenko, B. A. Piot, M. Orlita, C. Consejo, S. Ruffenach, W. Knap, A. Nateprov, E. Arushanov, and F. Teppe, Phys. Rev. B **97**, 245203 (2018).

[22] B.-J. Yang and N. Nagaosa, Nat. Commun. **5**, 4898 (2014).

[23] Z. K. Liu, J. Jiang, B. Zhou, Z. J. Wang, Y. Zhang, H. M. Weng, D. Prabhakaran, S.-K. Mo, H. Peng, P. Dudin, T. Kim, M. Hoesch, Z. Fang, X. Dai, Z. X. Shen, D. L. Feng, Z. Hussain, and Y. L. Chen, Nat. Mater. **13**, 677 (2014).

[24] S. Jeon, B. B. Zhou, A. Gyenis, B. E. Feldman, I. Kimchi, A. C. Potter, Q. D. Gibson, R. J. Cava, A. Vishwanath, and A. Yazdani, Nat. Mater. **13**, 851 (2014).

[25] S. Borisenko, Q. Gibson, D. Evtushinsky, V. Zabolotnyy, B. Büchner, and R. J. Cava, Phys. Rev. Lett. **113**, 027603 (2014).

[26] M. Neupane, S.-Y. Xu, R. Sankar, N. Alidoust, G. Bian, C. Liu, I. Belopolski, T.-R. Chang, H.-T. Jeng, H. Lin, A. Bansil, F. Chou, and M. Z. Hasan, Nat. Commun. **5**, 3786 (2014).

[27] T. Liang, J. Lin, Q. Gibson, T. Gao, M. Hirschberger, M. Liu, R. J. Cava, and N. P. Ong, Phys. Rev. Lett. **118**, 136601 (2017).

[28] M. Uchida, Y. Nakazawa, S. Nishihaya, K. Akiba, M. Kriener, Y. Kozuka, A. Miyake, Y. Taguchi, M. Tokunaga, N. Nagaosa *et al.*, Nat. Commun. **8**, 2274 (2017).

[29] T. Schumann, L. Galletti, D. A. Kealhofer, H. Kim, M. Goyal, and S. Stemmer, Phys. Rev. Lett. **120**, 016801 (2018).

[30] C.-Z. Li, L.-X. Wang, H. Liu, J. Wang, Z.-M. Liao, and D.-P. Yu, Nat. Commun. **6**, 10137 (2015).

[31] P. J. W. Moll, N. L. Nair, T. Helm, A. C. Potter, I. Kimchi, A. Vishwanath, and J. G. Analytis, Nature (London) **535**, 266 (2016).

[32] Z. Jia, C. Li, X. Li, J. Shi, Z. Liao, D. Yu, and X. Wu, Nat. Commun. **7**, 13013 (2016).

[33] M. Wu, G. Zheng, W. Chu, Y. Liu, W. Gao, H. Zhang, J. Lu, Y. Han, J. Zhou, W. Ning, and M. Tian, Phys. Rev. B **98**, 161110 (2018).

[34] A. Pietraszko and K. Lukaszewicz, Phys. Status Solidi A **18**, 723 (1973).

[35] E. Arushanov, Prog. Cryst. Growth Charact. **3**, 211 (1980).

[36] S. Jandl, S. Desgreniers, C. Carlone, and M. J. Aubin, J. Raman Spectrosc. **15**, 137 (1984).

[37] D. Neubauer, J. P. Carbotte, A. A. Nateprov, A. Löhle, M. Dressel, and A. V. Pronin, Phys. Rev. B **93**, 121202 (2016).

[38] D. Houde, S. Jandl, M. Banville, and M. Aubin, Solid State Commun. **57**, 247 (1986).

[39] G. A. Silvey, V. J. Lyons, and V. J. Silvestri, J. Electrochem. Soc. **108**, 653 (1961).

[40] S. E. R. Hiscocks and C. T. Elliott, J. Mater. Sci. **4**, 784 (1969).

[41] L. Zdanowicz, Phys. Status Solidi B **6**, K153 (1964).

[42] J. Pawlikowski, K. Sierański, and J. Szatkowski, Thin Solid Films **30**, 99 (1975).

[43] J. J. Dubowski and D. F. Williams, Appl. Phys. Lett. **44**, 339 (1984).

[44] E. Arushanov, Prog. Cryst. Growth Charact. **25**, 131 (1992).

[45] A. Akrap, M. Hakl, S. Tchoumakov, I. Crassee, J. Kuba, M. O. Goerbig, C. C. Homes, O. Caha, J. Novák, F. Teppe, W. Desrat, S. Koohpayeh, L. Wu, N. P. Armitage, A. Nateprov, E. Arushanov, Q. D. Gibson, R. J. Cava, D. van der Marel, B. A. Piot *et al.*, Phys. Rev. Lett. **117**, 136401 (2016).

[46] R. Sankar, M. Neupane, S.-Y. Xu, C. Butler, I. Zeljkovic, I. P. Muthuselvam, F.-T. Huang, S.-T. Guo, S. K. Karna, M.-W. Chu *et al.*, Sci. Rep. **5**, 12966 (2015).

[47] M. H. Weiler, in *Defects, (HgCd)Se, (HgCd)Te, Semiconductors and Semimetals*, edited by R. K. Willardson and A. C. Beer (Elsevier, Amsterdam, 1981), Vol. 16, pp. 119–191.

[48] P. Y. Yu and M. Cardona, *Fundamentals of Semiconductors* (Springer, Berlin, 2010).

[49] D. P. Spitzer, G. A. Castellion, and G. Haacke, J. Appl. Phys. **37**, 3795 (1966).

[50] A. Rambo and M. J. Aubin, Can. J. Phys. **57**, 2093 (1979).

[51] I. Crassee, E. Martino, C. C. Homes, O. Caha, J. Novák, P. Tückmantel, M. Hakl, A. Nateprov, E. Arushanov, Q. D. Gibson, R. J. Cava, S. M. Koohpayeh, K. E. Arpino, T. M. McQueen, M. Orlita, and A. Akrap, Phys. Rev. B **97**, 125204 (2018).

[52] H. Schleijpen, M. von Ortenberg, M. Gelten, and F. Blom, Int. J. Infrared Milli. **5**, 171 (1984).

[53] L.-X. Wang, C.-Z. Li, D.-P. Yu, and Z.-M. Liao, Nat. Commun. **7**, 10769 (2016).

[54] X. Yuan, P. Cheng, L. Zhang, C. Zhang, J. Wang, Y. Liu, Q. Sun, P. Zhou, D. W. Zhang, Z. Hu, X. Wan, H. Yan, Z. Li, and F. Xiu, Nano Lett. **17**, 2211 (2017).

[55] L. Galletti, T. Schumann, O. F. Shoron, M. Goyal, D. A. Kealhofer, H. Kim, and S. Stemmer, Phys. Rev. B **97**, 115132 (2018).

[56] E. D. Haidemenakis, M. Balkanski, E. D. Palik, and J. Tavernier, in *Proceedings Inst. Conf. Semiconductors, Kyoto*,

edited by G. M. Hatoyama (The Physical Society of Japan, 1966), p. 189.

[57] N. Sexer, Phys. Status Solidi B **21**, 225 (1967).

[58] E. O. Kane, J. Phys. Chem. Solids **1**, 249 (1957).

[59] R. Bowers and Y. Yafet, Phys. Rev. **115**, 1165 (1959).

[60] C. R. Pidgeon and R. N. Brown, Phys. Rev. **146**, 575 (1966).

[61] M. J. Aubin, L. G. Caron, and J. P. Jay-Gerin, Phys. Rev. B **15**, 3872 (1977).

[62] J. P. Jay-Gerin and A. A. Lakhani, J. Low Temp. Phys. **28**, 15 (1977).

[63] P. Kacman and W. Zawadzki, Phys. Status Solidi B **47**, 629 (1971).

[64] M. Orlita, D. M. Basko, M. S. Zholudev, F. Teppe, W. Knap, V. I. Gavrilenko, N. N. Mikhailov, S. A. Dvoretskii, P. Neugebauer, C. Faugeras, A.-L. Barra, G. Martinez, and M. Potemski, Nat. Phys. **10**, 233 (2014).

[65] J. D. Malcolm and E. J. Nicol, Phys. Rev. B **92**, 035118 (2015).

[66] F. Teppe, M. Marcinkiewicz, S. S. Krishtopenko, S. Ruffenach, C. Consejo, A. M. Kadykov, W. Desrat, D. But, W. Knap, J. Ludwig, S. Moon, D. Smirnov, M. Orlita, Z. Jiang, S. V. Morozov, V. I. Gavrilenko, N. N. Mikhailov, and S. A. Dvoretskii, Nat. Commun. **7**, 12576 (2016).

[67] A. M. Conte, O. Pulci, and F. Bechstedt, Sci. Rep. **7**, 45500 (2017).

[68] H. Kildal, Phys. Rev. B **10**, 5082 (1974).

[69] P. R. Wallace, Phys. Status Solidi B **92**, 49 (1979).

[70] M. Singh and P. R. Wallace, J. Phys. C: Solid State Phys. **16**, 3877 (1983).

[71] M. Singh, P. R. Wallace, and J. Leotin, J. Phys. C: Solid State Phys. **17**, 1385 (1984).

[72] P. J. Lin-Chung, Phys. Rev. **188**, 1272 (1969).

[73] P. J. Lin-Chung, Phys. Status Solidi B **47**, 33 (1971).

[74] B. Dowgiałło-Plenkiewicz and P. Plenkiewicz, Phys. Status Solidi B **94**, K57 (1979).

[75] K. Sierański, J. Szatkowski, and J. Misiewicz, Phys. Rev. B **50**, 7331 (1994).

[76] N. M. Shchelkachev and V. G. Yarzhemsky, Inorg. Mater. **54**, 1093 (2018).

[77] M. Hakl, S. Tchoumakov, I. Crassee, A. Akrap, B. A. Piot, C. Faugeras, G. Martinez, A. Nateprov, E. Arushanov, F. Teppe, R. Sankar, W.-l. Lee, J. Debray, O. Caha, J. Novák, M. O. Goerbig, M. Potemski, and M. Orlita, Phys. Rev. B **97**, 115206 (2018).

[78] Y. Zhao, H. Liu, C. Zhang, H. Wang, J. Wang, Z. Lin, Y. Xing, H. Lu, J. Liu, Y. Wang, S. M. Brombosz, Z. Xiao, S. Jia, X. C. Xie, and J. Wang, Phys. Rev. X **5**, 031037 (2015).

[79] H. Yi, Z. Wang, C. Chen, Y. Shi, Y. Feng, A. Liang, Z. Xie, S. He, J. He, Y. Peng, X. Liu, Y. Liu, L. Zhao, G. Liu, X. Dong, J. Zhang, M. Nakatake, M. Arita, K. Shimada, H. Namatame *et al.*, Sci. Rep. **4**, 6106 (2014).

[80] S. Roth, H. Lee, A. Sterzi, M. Zacchigna, A. Politano, R. Sankar, F. C. Chou, G. Di Santo, L. Petaccia, O. V. Yazyev, and A. Crepaldi, Phys. Rev. B **97**, 165439 (2018).

[81] A. C. Potter, I. Kimchi, and A. Vishwanath, Nat. Commun. **5**, 5161 (2014).

[82] M. Kargarian, M. Randeria, and Y.-M. Lu, Proc. Natl. Acad. Sci. USA **113**, 8648 (2016).

[83] C. J. Butler, Y. Tseng, C.-R. Hsing, Y.-M. Wu, R. Sankar, M.-F. Wang, C.-M. Wei, F.-C. Chou, and M.-T. Lin, Phys. Rev. B **95**, 081410 (2017).

[84] L. Zdanowicz, Phys. Status Solidi B **20**, 473 (1967).

[85] R. J. Wagner, E. D. Palik, and E. M. Swiggard, J. Phys. Chem. Solids Suppl. **1**, 471 (1971).

[86] P. L. Radoff and S. G. Bishop, Phys. Rev. B **5**, 442 (1972).

[87] M. Gelten, C. van Es, F. Blom, and J. Jongeneelen, Solid State Commun. **33**, 833 (1980).

[88] M. J. Aubin, A. Rambo, and E. Arushanov, Phys. Rev. B **23**, 3602 (1981).

[89] J.-P. Jay-Gerin, K. Arushanov, and M. Aubin, Solid State Commun. **46**, 537 (1983).

[90] M. Singh and P. Wallace, Physica B&C (Amsterdam) **117-118**, 441 (1983).

[91] H. E. A. Lamrani and M. Aubin, Can. J. Phys. **65**, 199 (1987).

[92] G. S. Jenkins, C. Lane, B. Barbiellini, A. B. Sushkov, R. L. Carey, F. Liu, J. W. Krizan, S. K. Kushwaha, Q. Gibson, T.-R. Chang, H.-T. Jeng, H. Lin, R. J. Cava, A. Bansil, and H. D. Drew, Phys. Rev. B **94**, 085121 (2016).

[93] E. Uykur, R. Sankar, D. Schmitz, and C. A. Kuntscher, Phys. Rev. B **97**, 195134 (2018).

[94] E. Burstein, Phys. Rev. **93**, 632 (1954).

[95] C. P. Weber, E. Arushanov, B. S. Berggren, T. Hosseini, N. Kouklin, and A. Nateprov, Appl. Phys. Lett. **106**, 231904 (2015).

[96] A. Sharafeev, V. Gnezdilov, R. Sankar, F. C. Chou, and P. Lemmens, Phys. Rev. B **95**, 235148 (2017).

[97] C. Zhu, X. Yuan, F. Xiu, C. Zhang, Y. Xu, R. Zhang, Y. Shi, and F. Wang, Appl. Phys. Lett. **111**, 091101 (2017).

[98] W. Lu, S. Ge, X. Liu, H. Lu, C. Li, J. Lai, C. Zhao, Z. Liao, S. Jia, and D. Sun, Phys. Rev. B **95**, 024303 (2017).

[99] W. Lu, J. Ling, F. Xiu, and D. Sun, Phys. Rev. B **98**, 104310 (2018).

[100] P. Goswami and S. Chakravarty, Phys. Rev. Lett. **107**, 196803 (2011).

[101] T. Timusk, J. P. Carbotte, C. C. Homes, D. N. Basov, and S. G. Sharapov, Phys. Rev. B **87**, 235121 (2013).

[102] I. Rosenman, Phys. Lett. **21**, 148 (1966).

[103] W. Zdanowicz, L. Zdanowicz, J. Portal, and S. Askenazy, Thin Solid Films **61**, 41 (1979).

[104] A. Narayanan, M. D. Watson, S. F. Blake, N. Bruyant, L. Drigo, Y. L. Chen, D. Prabhakaran, B. Yan, C. Felser, T. Kong, P. C. Canfield, and A. I. Coldea, Phys. Rev. Lett. **114**, 117201 (2015).

[105] S.-T. Guo, R. Sankar, Y.-Y. Chien, T.-R. Chang, H.-T. Jeng, G.-Y. Guo, F. Chou, and W.-L. Lee, Sci. Rep. **6**, 27487 (2016).

[106] Z. J. Xiang, D. Zhao, Z. Jin, C. Shang, L. K. Ma, G. J. Ye, B. Lei, T. Wu, Z. C. Xia, and X. H. Chen, Phys. Rev. Lett. **115**, 226401 (2015).

[107] J. Feng, Y. Pang, D. Wu, Z. Wang, H. Weng, J. Li, X. Dai, Z. Fang, Y. Shi, and L. Lu, Phys. Rev. B **92**, 081306 (2015).

[108] A. A. Abrikosov, J. Phys. A: Math. Gen. **36**, 9119 (2003).

[109] H. Li, H. He, H.-Z. Lu, H. Zhang, H. Liu, R. Ma, Z. Fan, S.-Q. Shen, and J. Wang, Nat. Commun. **7**, 10301 (2016).

[110] R. D. dos Reis, M. O. Ajeesh, N. Kumar, F. Arnold, C. Shekhar, M. Naumann, M. Schmidt, M. Nicklas, and E. Hassinger, New J. Phys. **18**, 085006 (2016).

[111] S. Liang, J. Lin, S. Kushwaha, J. Xing, N. Ni, R. J. Cava, and N. P. Ong, Phys. Rev. X **8**, 031002 (2018).

[112] L. P. He, X. C. Hong, J. K. Dong, J. Pan, Z. Zhang, J. Zhang, and S. Y. Li, Phys. Rev. Lett. **113**, 246402 (2014).

[113] W. Desrat, C. Consejo, F. Teppe, S. Contreras, M. Marcinkiewicz, W. Knap, A. Nateprov, and E. Arushanov, J. Phys.: Conf. Ser. **647**, 012064 (2015).

[114] A. Pariari, P. Dutta, and P. Mandal, Phys. Rev. B **91**, 155139 (2015).

[115] G. P. Mikitik and Y. V. Sharlai, Phys. Rev. B **67**, 115114 (2003).

[116] F. Blom, J. Cremers, J. Neve, and M. Gelten, Solid State Commun. **33**, 69 (1980).

[117] L.-P. He and S.-Y. Li, Chin. Phys. B **25**, 117105 (2016).

[118] P. Cheng, C. Zhang, Y. Liu, X. Yuan, F. Song, Q. Sun, P. Zhou, D. W. Zhang, and F. Xiu, New J. Phys. **18**, 083003 (2016).

[119] K. S. Novoselov, A. K. Geim, S. V. Morozov, D. Jiang, M. I. Katsnelson, I. V. Grigorieva, S. V. Dubonos, and A. A. Firsov, Nature (London) **438**, 197 (2005).

[120] I. A. Luk'yanchuk and Y. Kopelevich, Phys. Rev. Lett. **93**, 166402 (2004).

[121] I. A. Luk'yanchuk and Y. Kopelevich, Phys. Rev. Lett. **97**, 256801 (2006).

[122] J. M. Schneider, M. Orlita, M. Potemski, and D. K. Maude, Phys. Rev. Lett. **102**, 166403 (2009).

[123] I. A. Luk'yanchuk and Y. Kopelevich, Phys. Rev. Lett. **104**, 119701 (2010).

[124] J. M. Schneider, M. Orlita, M. Potemski, and D. K. Maude, Phys. Rev. Lett. **104**, 119702 (2010).

[125] C. Zhang, A. Narayan, S. Lu, J. Zhang, H. Zhang, Z. Ni, X. Yuan, Y. Liu, J.-H. Park, E. Zhang *et al.*, Nat. Commun. **8**, 1272 (2017).

[126] H. Li, H.-W. Wang, H. He, J. Wang, and S.-Q. Shen, Phys. Rev. B **97**, 201110 (2018).